



Mechanical properties and acoustic emission characteristics of soft rock with different water contents under dynamic disturbance

Yujing Jiang¹ · Lugen Chen¹ · Dong Wang^{1,2} · Hengjie Luan^{1,3} · Guangchao Zhang¹ · Ling Dong¹ · Bin Liang¹

Received: 27 April 2023 / Revised: 9 August 2023 / Accepted: 11 March 2024
© The Author(s) 2024

Abstract

Uniaxial compression tests and cyclic loading acoustic emission tests were conducted on 20%, 40%, 60%, 80%, dry and saturated muddy sandstone by using a creep impact loading system to investigate the mechanical properties and acoustic emission characteristics of soft rocks with different water contents under dynamic disturbance. The mechanical properties and acoustic emission characteristics of muddy sandstones at different water contents were analysed. Results of experimental studies show that water is a key factor in the mechanical properties of rocks, softening them, increasing their porosity, reducing their brittleness and increasing their plasticity. Under uniaxial compression, the macroscopic damage characteristics of the muddy sandstone change from mono-bevel shear damage and ‘X’ type conjugate bevel shear damage to a roadway bottom-drum type damage as the water content increases. Dynamic perturbation has a strengthening effect on the mechanical properties of samples with 60% and less water content, and a weakening effect on samples with 80% and more water content, but the weakening effect is not obvious. Macroscopic damage characteristics of dry samples remain unchanged, water samples from shear damage and tensile–shear composite damage gradually transformed into cleavage damage, until saturation transformation monoclinic shear damage. The evolution of acoustic emission energy and event number is mainly divided into four stages: loading stage (I), dynamic loading stage (II), yield failure stage (III), and post-peak stage (IV), the acoustic emission characteristics of the stages were different for different water contents. The characteristic value of acoustic emission key point frequency gradually decreases, and the damage degree of the specimen increases, corresponding to low water content—high main frequency—low damage and high water content—low main frequency—high damage.

Keywords Dynamic disturbance · Soft rock · Cyclic loading · Acoustic emission · Water content

1 Introduction

Deep mining has gradually become the new normal for coal resource development in China along with their increase in demand and the depletion of shallow resources (Xie

et al. 2015; Wang et al. 2022; Zhang et al. 2023; Huang et al. 2020). In deep soft rock mines, soft rock roadways exhibit significant creep characteristics, such as nonlinear large deformation and long duration of deformation (He et al. 2005). In complex geological conditions, coal mining results in damage to the structure and integrity of the overlying rock formations and the diversion of water resources (Sun et al. 2021). The physicochemical interaction between water and rock not only changes the mineral composition and microstructure of the rock, but also affects the mechanical properties and deformation characteristics of the rock. These important factors deteriorate the mechanical properties of the rock (Wong et al. 2015; Li et al. 2019; Zhou et al. 2022). Deep soft rock mines are in a geological environment of ‘three highs and one disturbance’, resulting in a more complex deformation and destabilisation mechanism of deep soft rock mine tunnels and seriously affecting the safe and efficient mining of deep soft rock mines in China.

✉ Dong Wang
wdwinter@163.com

¹ State Key Laboratory of Mining Disaster Prevention and Control Co-Founded By Shandong Province and the Ministry of Science and Technology, Shandong University of Science and Technology, Qingdao 266590, China

² State Key Laboratory for Geomechanics and Deep Underground Engineering, China University of Mining and Technology, Beijing 100083, China

³ Inner Mongolia Shanghaimiao Mining Co., Ltd., Ordos 016299, China

In a current study of deep water-rich soft rocks, Erguler and Ulusay (2008) found that the strength index of clayey soft rocks was reduced by more than 90% in the saturated state compared with that of dry rocks. Roy et al. (2017) studied the effect of different water saturation times on the mechanical parameters of sandstone and found that the tensile strength, Young's modulus and fracture stiffness of sandstone decreased with increasing water content. Sun et al. (2023) carried out creep experiments on sandstones with different water contents and concluded that the damage form of rock samples would change from single-sided shear to 'X' type conjugate shear as the water content increases. Liu et al. (2020) investigated the strength characteristics of frozen sandstones with different initial water contents and concluded that the uniaxial compressive strength of water-bearing sandstone specimens increased linearly with decreasing freezing temperature. Yu et al. (2019) and Tang et al. (2018) carried out uniaxial compression creep tests on red sandstone with different water contents and found that the instantaneous and steady-state strain rates increased exponentially with increasing water content. Zhang et al. (2021a, b) A thermal shock damage ontological model was proposed, laying the foundation for the study of thermal damage in rocks.

In the studies on the dynamic response of rocks, impact tests were carried out on rocks of different lithologies (Cai et al. 2020; Weng et al. 2020; Gao et al. 2018; Zhao et al. 2016). Yang et al. (2022) analysed water-bearing sandstone under cyclic loading and concluded that the axial deformation of rock samples decreased with increasing water content. Xu et al. (2006; Xi et al. 2003; Liu and He (2012) investigated the effects of upper limit stress, cyclic amplitude, cyclic frequency and loading waveform on cyclic loading and unloading of rocks. Zhao et al. (2019) used cyclic loading and seepage experiments to derive the law that the

permeability of sandstones gradually increases when the cyclic loading increases step by step. Feng et al. (2022) used the finite element combination method to simulate the damage process of underground cavern, revealing the damage mechanism of deep hard rock affected by the dynamic stress amplitude, disturbance direction, and structural surface inclination angle. Some studies (Zhang et al. 2006; Xiao et al. 2010; Li et al. 2009; Guo et al. 2011) investigated the damage process of rocks under cyclic action from different perspectives.

In summary, most scholars only study the static load mechanical characteristics or creep characteristics of soft rocks under the action of water, and studies combining the dynamic response of rocks with the action of water are relatively few, but their impact is significant. Therefore, the mechanical characteristics of soft rocks with different water contents under the action of dynamic disturbance should be studied, and the deformation and instability rules of soft rock roadways in deep soft rock mines in China should be explored to ensure long-term stability and safe and efficient mining in deep soft rock mines in China.

2 Experimental scheme and conditions

2.1 Experimental system

The experimental test rig consists of a creep dynamic disturbance impact loading system and an acoustic emission acquisition system. As shown in Fig. 1, the system works by driving the hydraulic oil from the oil pump into the accumulator by means of a servo motor and controlling the axial movement of the double piston rod structure in the accumulator with the input of the hydraulic oil into the power chamber with the aid of a high-frequency ringing dynamic

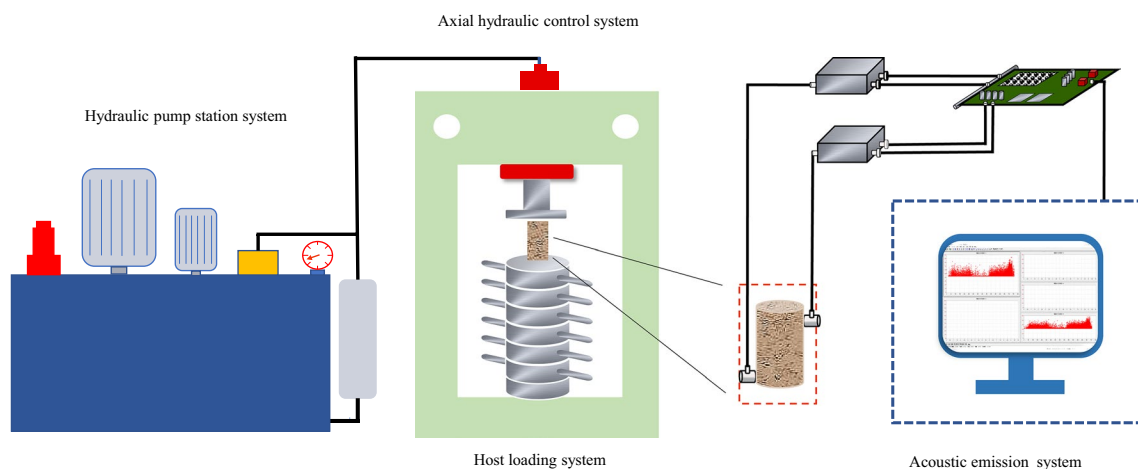


Fig. 1 Dynamic impact loading simulation test system for creep disturbance

servo valve. The static loading unit in the loading system of the experimental host has a vertical load of 0–800 kN, the maximum vertical load of the dynamic loading unit is 100 kN, and the maximum stroke of the actuator is 150 mm. The static load displacement rate ranges from 0.1 to 150.0 mm/min, and the dynamic load displacement rate ranges from 0.05 to 100.00 mm/min, and the measurement accuracy can be up to $\pm 0.5\%$ of the displayed value. The system is capable of realising composite waveform loading including sinusoidal waveform, rectangular waveform and custom waveform, and the disturbance frequency of these disturbed waveforms ranges from 0.01 to 10.00 Hz. Acoustic emission acquisition system for the U.S. physical acoustic PAC (physical acoustic corporation) company's Sensor Highway II acoustic emission device can be collected A.E. events, energy, amplitude, and other A.E. characteristics of the parameter, the use of R15 α probe (response frequency range of 50–200 kHz), double probe arrangement. The acoustic emission probe was fixed at the diagonal of the specimen during the experiment, and a layer of petroleum jelly was uniformly applied between the acoustic emission probe and the monitoring surface of the specimen as a coupling agent to ensure a close fit between the sensor and the specimen. In order to eliminate the influence of noise on the experimental data, the threshold of the acoustic emission system was set to 43 dB, the sampling frequency was 1 MHz, the amplification of the preamplifier was 40 times, and the length of the acoustic emission signal was 1024. During the process of rock from compressional deformation to damage, the loading system always runs synchronously with the acoustic emission acquisition system.

2.2 Specimen preparation

In this experiment, a standard cylindrical rock sample of 50 mm diameter and 100 mm height was prepared in accordance with the International Society for Rock Mechanics (ISRM) experimental protocols. The muddy sandstone of New Shanghai No. 1 coal mine, without defects visible to the naked eye on the surface of the rock specimen, was used as the object of study. The end unevenness and axis imperfections were controlled within ± 0.02 mm to mitigate the end effect of the sandstone in this experiment.

The samples were divided into six groups: one dry group, four groups with water and one group full of water; each group has six samples, for a total of 36 samples. The samples were dried in a constant temperature blast oven (drying temperature set at 110° , drying time set at 12 h) to obtain the dried samples. The samples were then completely submerged after 6 h and allowed to absorb the water. The samples were removed at regular intervals, the surface water was wiped off, and their mass was measured until the mass no longer changed.

Figure 2 shows the variation curve of the water content of the rock sample with the soaking time. The figure indicates that the water content of the rock sample increases almost linearly with time during the first 5 h of immersion, with bubbles overflowing from the end face of the sample during the immersion process. As a result, the trend of water content change with soaking time can be divided into three stages: I water content rapid growth stage (0–5 h); II water content slow growth stage (5–12 h); III water content stable stage (12–24 h). After 24 h, the rock samples have reached saturation state when the water content of the rock samples show no evident change for 12 consecutive hours (24–36 h). The average saturated water content was 8.689% and was considered 100%. The remaining four sets of samples were made to contain 20%, 40%, 60% and 80% water and were stored in sealed bags in jars.

2.3 Test program

The experiment is divided into two parts: the first part aims to determine the static parameters of rock samples with different water contents, uniaxial damage characteristics and initial value of cyclic loading for uniaxial compression experiments, the experimental process of displacement-controlled loading at 0.1 mm/min loading speed, until the destruction of rock samples. The physical parameters of the experimental samples are shown in Table 1. The second part uses cyclic loading to simulate the effect of dynamic disturbance on the deep soft rock roadway. The waveform of disturbance is a sine wave, with frequency of 5 Hz, amplitude of $\Delta\sigma = 10$ kN, number of disturbance of 1000 times, cyclic loading and acoustic emission experiments under different static load σ_m . The experimental program of the samples

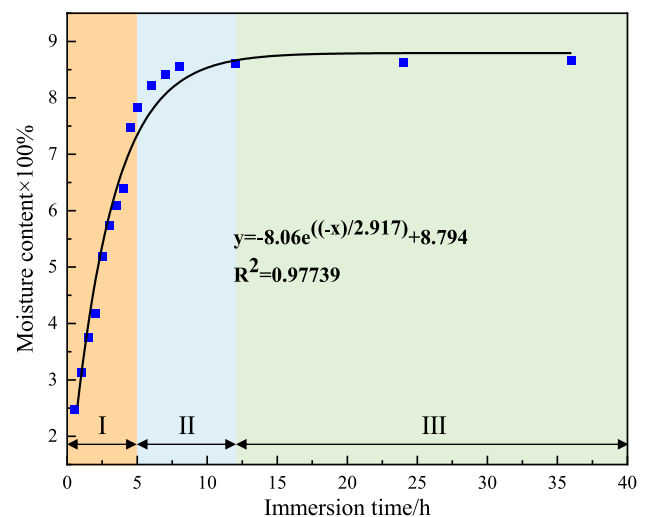


Fig. 2 Curve of water content over time

Table 1 Physical properties of siltstone under different water contents

State of rock sample	Rock sample number	Diameter (mm)	Height (mm)	Quality after drying (g)	Quality after immersion (g)	Water content (%)	Average water content (%)
Dryness	D0-1	50.23	100.07	412.910	–	0	0
	D0-2	50.40	100.30	413.477	–	0	
	D0-3	50.40	100.01	411.493	–	0	
20% water content	D2-1	50.32	100.12	411.776	419.714	1.927	2.005
	D2-2	50.24	99.83	411.493	419.714	1.997	
	D2-3	50.30	99.99	407.099	415.604	2.089	
40% water content	D4-1	50.18	99.91	407.099	421.699	3.586	3.453
	D4-2	50.42	100.01	412.343	426.235	3.368	
	D4-3	50.34	99.97	403.967	417.446	3.405	
60% water content	D6-1	50.32	100.00	407.524	428.219	5.078	5.060
	D6-2	50.34	100.21	415.887	436.866	5.044	
	D6-3	50.37	99.96	406.248	426.802	5.059	
80% water content	D8-1	50.21	100.12	409.509	438.000	6.957	6.956
	D8-2	50.13	100.00	410.501	438.992	6.940	
	D8-3	50.37	100.29	408.658	437.150	6.971	
Saturation	D10-1	50.10	100.25	412.911	448.773	8.685	8.689
	D10-2	50.27	99.88	407.383	442.820	8.698	
	D10-3	49.96	100.02	411.210	446.930	8.686	

Table 2 Experimental program of rock samples under dynamical disturbance

State of rock sample	Rock sample number	Water content (%)	Average water content (%)	σ_m (kN)	$\Delta\sigma$ (kN)	Frequency (Hz)	Number of disturbances
Dryness	R0-1	0	0	33.89	10	5	1000
	R0-2	0			10	5	1000
	R0-3	0			10	5	1000
20% water content	R2-1	1.863	1.820	17.90	10	5	1000
	R2-2	1.784			10	5	1000
	R2-3	1.813			10	5	1000
40% water content	R4-1	3.564	3.611	15.94	10	5	1000
	R4-2	3.492			10	5	1000
	R4-3	3.778			10	5	1000
60% water content	R6-1	5.254	5.283	15.28	10	5	1000
	R6-2	5.270			10	5	1000
	R6-3	5.327			10	5	1000
80% water content	R8-1	6.995	6.984	13.97	10	5	1000
	R8-2	6.957			10	5	1000
	R8-3	7.000			10	5	1000
Saturation	R10-1	8.636	8.679	12.99	10	5	1000
	R10-2	8.779			10	5	1000
	R10-3	8.621			10	5	1000

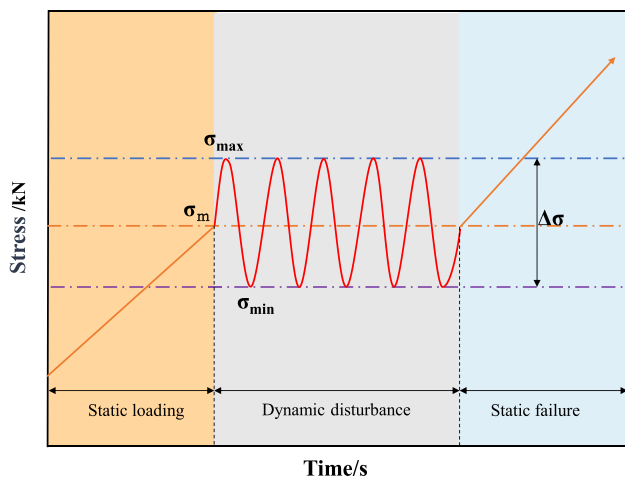


Fig.3 Schematic diagram of the loading process for cyclic disturbance loads

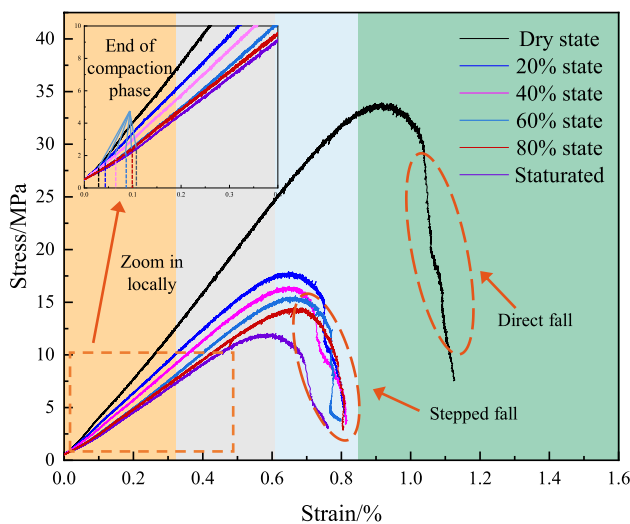


Fig.4 Uniaxial compression stress–strain curves

under dynamic disturbance is shown in Table 2. A schematic of the cyclic perturbation loading process is shown in Fig. 3.

3 Analysis of experimental results

3.1 Uniaxial compression experimental results

Uniaxial compression experiments were carried out on several groups of muddy sandstones with different water contents, and the uniaxial compression stress–strain curves of the samples with different water contents were obtained, as shown in Fig. 4. Figure 4 shows that the entire process of damage under uniaxial compression for each water content sample can be divided into the primary fracture

compaction stage, the linear elastic stage, the yielding stage, the damage stage and the post-damage stage. In the early stages of loading, the primary fracture compaction phase increases significantly with increasing water content, and the linear elastic phase decreases significantly. From the perspective of rock composition, the water content dissolves some of the cement between the internal particles of the rock, weakening the friction between the particles, coupled with the dissolving effect of water, causing micro-pores and micro-fractures to appear inside the rock. Moreover, the internal structure becomes loose, resulting in the growth of the compaction phase of the primary fracture of the rock curve and the reduction of the linear elastic phase. At the micro level, the rock is a non-homogeneous body, and many micro-voids are found inside the rock in its natural state. When comparing the post-peak stress–strain curves for each water content, the dry samples show a direct drop in brittleness after the peak. Furthermore, as the water content increases, the post-peak curves show varying degrees of stepwise stress rebound, with evident post-peak residual strength, indicating that the samples are gradually becoming less brittle and more plastic. The general trend of the stress–strain curves of the samples with different water contents is the same, but the peak strain and the stress growth rate of the samples decrease with increasing water content. This finding leads to the conclusion that water has a softening effect on the rock, increasing its porosity, decreasing its brittleness and increasing its plasticity.

The fitted uniaxial compressive strength and modulus of elasticity curves are shown in Fig. 5, where the strength and modulus of the samples with different water contents decrease to varying degrees with increasing water content. The average uniaxial compressive strengths of the samples in dry, 20%, 40%, 60% and 80% water and in saturated states were 34.485, 18.237, 16.236, 15.561, 14.349 and 13.234 MPa, respectively. In addition, using the saturated strength of 13.234 MPa as the base, the strengths of the rock samples in each state decreased by 60.79%, 28.58%, 18.49%, 14.95% and 7.00%. The modulus of elasticity was 4.146, 2.962, 2.836, 2.600, 2.343 and 2.311 GPa with a decrease of 44.26%, 21.98%, 18.51%, 11.12% and 1.36% in the modulus of elasticity of the rock samples, respectively, in each condition based on the saturated state modulus of elasticity of 2.311 GPa. As the water content increased, the uniaxial strength decreased from an initial 34.485–13.234 MPa, indicating a decrease of 62.62%, and the modulus of elasticity of the sandstone decreased from an initial 4.146–2.311 GPa, representing a decrease of 44.26%. The finding shows that water has a significant effect on the mechanical properties of the rock. The uniaxial compressive strength and modulus of elasticity of the samples in each state indicate a negative exponential relationship between the uniaxial compressive

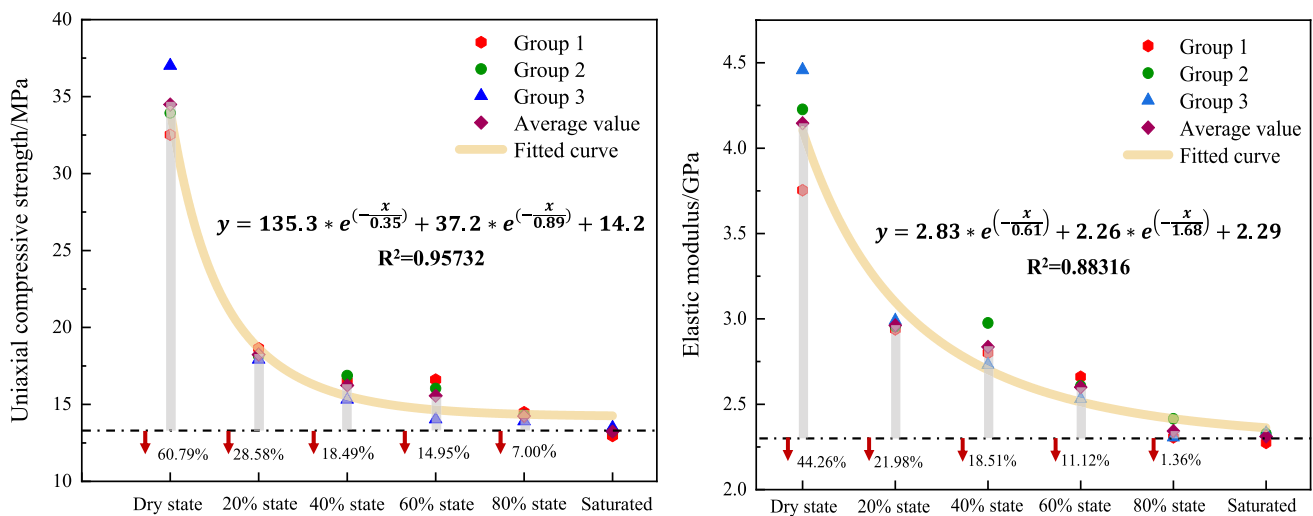


Fig.5 Variation of elastic modulus and compressive strength of argillaceous sandstone with different water content

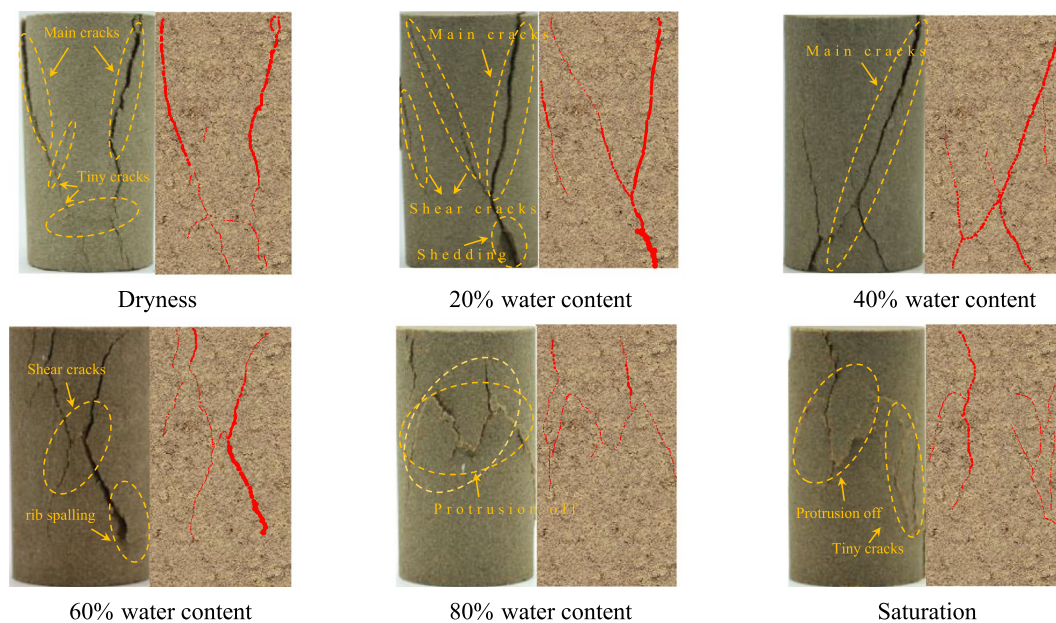


Fig.6 Variation of elastic modulus and compressive strength of argillaceous sandstone with different water content

strength and modulus of elasticity of the muddy sandstone and the water content, as shown in Fig. 5.

Figure 6 shows the damage characteristics of typical specimens under uniaxial compression of muddy sandstones with different water contents, as follows: (1) The dried sample consists of multiple axial cracks developed on the end face and extending to the bottom of the dried rock sample specimen, and multiple fine cracks developed in the extension path of the main crack, exhibiting an overall form of shear damage; (2) The main crack developed on the upper face of the 20% water sample penetrates the entire sample and forms

a shear break angle of approximately 60° on the surface of the sample, with small pieces of debris falling off during the experiment and microcracks developing on the surface of the sample almost parallel to the shear break fractures; (3) The 40% water sample shows more pronounced unilateral shear damage at a 60° shear angle, with more microfractures developing around the main fracture, greater damage to the sample and a tendency for rib spalling to form around the sample; (4) The 60% content sample consists of several axial fissures developed on the upper face and extending to the lower part of the sample. The fissures as a whole show

a clear 'X' shape, which is an 'X' type conjugate bevel shear damage. Moreover, the overall damage of the sample increases further, with evident signs of flake ganging; (5) Compared with the other samples, the 80% water-bearing rock samples did not develop through large cracks, and although the samples were subjected to axial stresses in the form of shear damage, they did not form a complete shear damage surface due to the 'softening' effect of water. In general, the sample exhibits macroscopic phenomena characterised by central protrusions and dislodgement-like roadway undercuts, with further damage; (6) The saturated samples are similar in form to the 80% water-bearing samples, but the saturated rock samples have a greater degree of protrusion and dislodgement, with more micro-cracks developed and more dramatic damage.

Therefore, the degree of damage to the muddy sandstone increases as the water content increases, and the macroscopic form of damage to the rock changes from the traditional single bevel shear damage and 'X' type conjugate bevel shear damage to a tunnel bottom drum type of damage as the water content approaches saturation. Therefore, as the water content of the surrounding rock in water-rich soft rock mines increases, the occurrence of roadway undercuts is greatly increased.

3.2 Analysis of the results of the dynamic disturbance experiments

During the experiment, graphs of cyclic disturbance loads, displacements and strains, as a function of time, can be measured directly. Initially, the axial static load is slowly applied to σ_m , followed by the predetermined experimental loading scheme with $\Delta\sigma$ stress amplitude cyclic loading. If the cycle can be completed, then the axial static load is

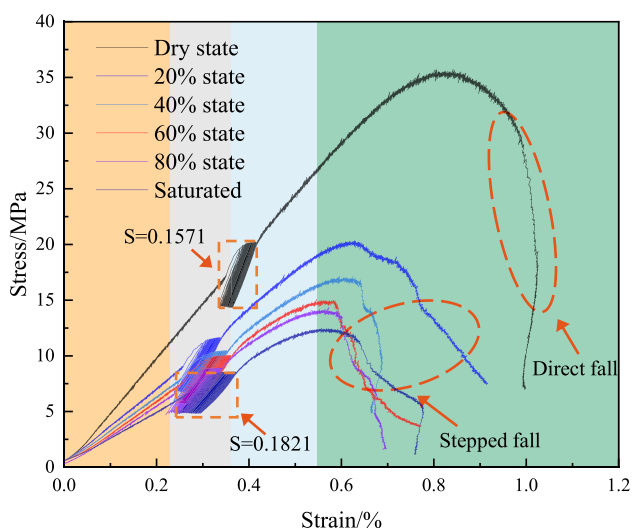


Fig.7 Disturbing stress–strain curve

continuously applied until the rock sample is damaged. The stress–strain curves for rocks with different water contents under disturbance are shown in Fig. 7, after discarding unreasonable data. The figure shows that the rock samples with different water contents completed 1000 cycles without damage, indicating that the initial value of cyclic disturbance σ_m selected for this experiment did not exceed the upper stress threshold of the muddy sandstone. At the beginning of loading, the slope of the stress–strain curve and the rate of stress growth showed a negative correlation with the water content. The stress–strain curve shows a sharp lobe-shaped hysteresis loop as the number of cycles increases, and the area of this hysteresis loop indicates the amount of energy lost during the cyclic disturbance. As can be seen in Fig. 7, the cumulative hysteresis loop area S (dimensionless quantity) of the dry sample is significantly smaller than that of the saturated sample because the internal particle brittleness of the sample is enhanced after drying, and some cement between the particles loses water and hardens, resulting in the continuous compaction and closure of the internal primary fractures during the cyclic disturbance of the sample. This condition restores the load-bearing capacity to a certain extent and results in a relatively small amount of internal energy loss dissipation. The saturated sample is filled with water due to the internal primary fissures, and some cement between the particles is dissolved in water to form a micro-water cavity. In the cyclic disturbance process, the hydrostatic pressure inside the contracting cavity of the micro-water cavity constantly changes and rises, resulting in the expansion of micro-cracks inside the sample. In general, the sample becomes flimsy, and the energy loss dissipation is relatively large. This finding explains the increase of 6.90%, 13.83%, 10.96% and 7.29% in the dry, 20% water, 40% water and 60% water perturbation strengths, respectively, in the uniaxial strength versus dynamic perturbation strength plot in Fig. 8, whereas the 80% water and saturated sample perturbation strength decreases by 0.49% and 2.47%. It can be concluded that the compressive strength of the low water content samples was strengthened by the dynamic disturbance, with the greatest strengthening of the samples at about 20% water content, which was as high as 13.83%. With the increase of water content, the strengthening effect of the disturbance on the samples gradually decreases, and 80% water content and above shows a weakening effect. This is due to the fact that when the sample is in 20% water content, the water in the sample exists in the form of bound water, and the erosion and hydration of bound water on the rock makes the cohesion between the internal particles of the rock sample decrease, which then leads to the lower uniaxial strength, but under the action of dynamic disturbance, the internal particles are re-compacted and densely compacted, and the cohesion between the internal particles of the sample and the load-bearing capacity of the sample have been

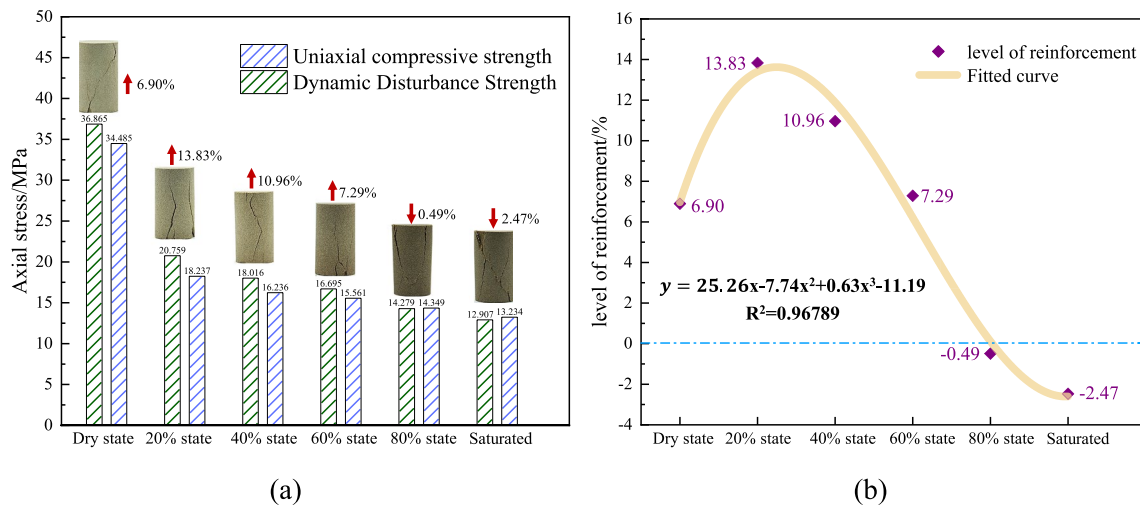


Fig.8 Comparison of strength of uniaxial compression and dynamic disturbance

restored to a certain extent. With the increase of water content, the content of free water in the internal microporous space of the sample gradually increased, and the water pressure of the microporous space under the action of dynamic perturbation constantly changed and rupture occurred. The higher the water content, the higher the free water content in the sample, the higher the number of microporous rupture, and the lower the compressive strength of the sample.

The damage pattern of different water-bearing samples is different, and the typical damage pattern of the samples selected for each state is shown in Fig. 9. The figure shows the following: (1) Damage to dry samples by kinetic disturbance is exhibited in the form of a main fissure developing at an angle of approximately 60° from the base through the top of the sample, where microcracks emerge and a small amount of debris is dislodged; the damage is manifested as

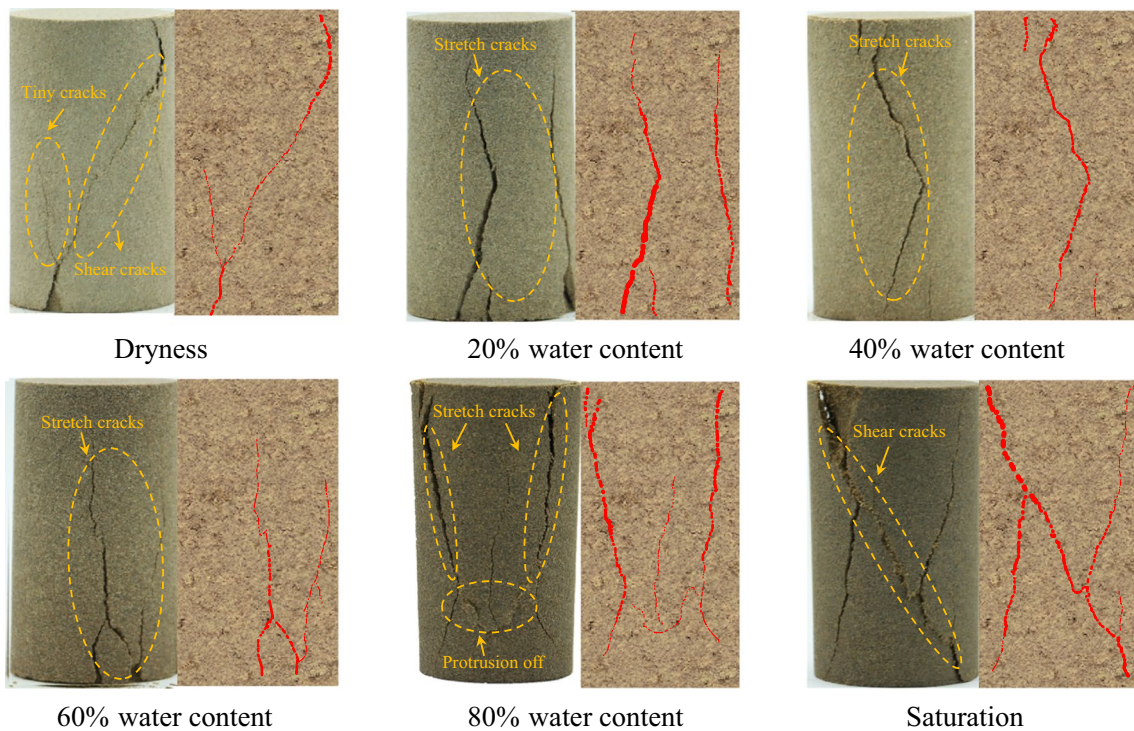


Fig.9 Macroscopic damage characteristics of samples with different water contents

monoclinic shear damage; (2) The damage of the 20% water-bearing sample is exhibited in the form of two main cracks almost parallel to the loading direction, with some debris loss at the bottom of the sample and a tendency of conical damage, showing overall tensile–shear compound damage; (3) Damage to the 40% water-bearing sample is in the form of a main fracture developing at an angle of approximately 60° to the top of the sample, to the middle of the sample and extending at an angle of approximately 60° to the bottom, showing splitting damage; (4) The 60% water-bearing samples show overall splitting damage from the main tensile crack developed at the base extending to the middle of the sample with small pieces of debris dislodged; (5) The 80% water content samples as two main cracks parallel to the loading direction developing from the top and extending towards the bottom, with the middle and bottom specimens showing signs of splitting damage by bulging off; (6) The saturated samples show the same form of damage as the dry samples, with monoclinic shear damage and more small fractures and debris loss.

Compared with uniaxial damage, the form of damage remains unchanged in the dry rock samples after disturbance, whereas the water-bearing rock samples change gradually from shear damage and tensile–shear composite damage with increasing water content to more pronounced cleavage damage until saturation after complete monoclinic shear damage.

3.3 Acoustic emission characteristics

The destructive process of various water-containing samples can be divided into four stages: static loading stage (I), dynamic loading stage (II), yield failure stage (III), and post-peak stage (IV). Different samples generate distinct acoustic emission signals during this process. Acoustic emission ring counts (the number of oscillations where the acoustic emission signal exceeds a certain set threshold) and energy (the area under the envelope of the acoustic emission signal) accurately reflect the intensity and frequency of the acoustic emission signals. Thus, they are commonly used to analyze the deformation and failure processes of samples during loading.

The Fig. 10 shows the relationship between the acoustic emission ring counts, energy, and stress–strain curves of different water-containing samples under dynamic perturbation. From the figure, it can be observed that: During the static loading stage (I), the dried samples experience hardening due to the loss of water in the particles and cementitious materials. As the sample is loaded, pre-existing cracks are repressed, and there is friction between particles, resulting in a higher count and magnitude of acoustic emission signals during this stage. As the water content increases, both the intensity and quantity of acoustic emission signals during

the static loading stage decrease. This is because water acts as a lubricant, reducing the friction between particles in the rock sample. Water also hinders the propagation of acoustic emission signals in the sample, leading to some signals not exceeding the set threshold of 43 dB and being filtered out as noise; During the dynamic loading stage (II), the axial load undergoes sudden changes, leading to a cyclic strengthening effect in the sample (Wen et al. 2021). As the number of cycles increases, the rate of internal microcrack propagation in the sample also increases. This results in a significant increase in acoustic emission signals, which gradually decreases and stabilizes with the increase in the number of cycles. The samples with higher water content (80% and above) exhibit a sudden change in acoustic emission energy and count signals during the perturbation stage. This is because in samples with higher water content, the water mainly exists as free water, and the interaction of free water with the water film in the internal cracks creates pore water pressure. During the perturbation process, the pore water pressure varies with the same frequency as the dynamic loading, causing the pores to continuously lose their bearing capacity and rupture, resulting in the phenomenon of sudden changes in acoustic emission signals during the perturbation stage; In the yield and failure stages (III), the change patterns of acoustic emission signals are similar for all water-containing samples. With the increase of axial stress, cracks in the sample continuously develop, and microcracks propagate and connect with each other until macroscopic cracks appear, penetrating the entire sample. During this period, acoustic emission signals continuously and steadily increase until the cracks penetrate the sample, causing a peak. The peak acoustic emission energy signals of the samples with different water contents were 21,402, 18,927, 8875, 2351, 743, and 117, and the ringing counts were 4739, 4502, 1563, 1245, and 172, respectively, and the acoustic emission signals decreased by multiplicative order of magnitude with the increase of water content.; In the post-peak stage (IV), dried samples do not exhibit significant signal generation after the peak, demonstrating brittle characteristics with instantaneous failure. On the other hand, other water-containing samples show different degrees of rebound in acoustic emission signals after the peak, indicating plastic characteristics with creep failure.

The specimen produces a continuous random signal of acoustic emission during the combined dynamic and static loading process. The acoustic emission signal is transformed from the time domain to the frequency domain by the fast Fourier transform, and the acoustic emission signal is formed into a waveform file every 1024 number lines, and the amplitude–frequency–time 3D map is obtained by Matlab. This section reflects the degree of damage to the sample by selecting a key point and by the variation of the high and low dominant frequency eigenvalues in the 3D

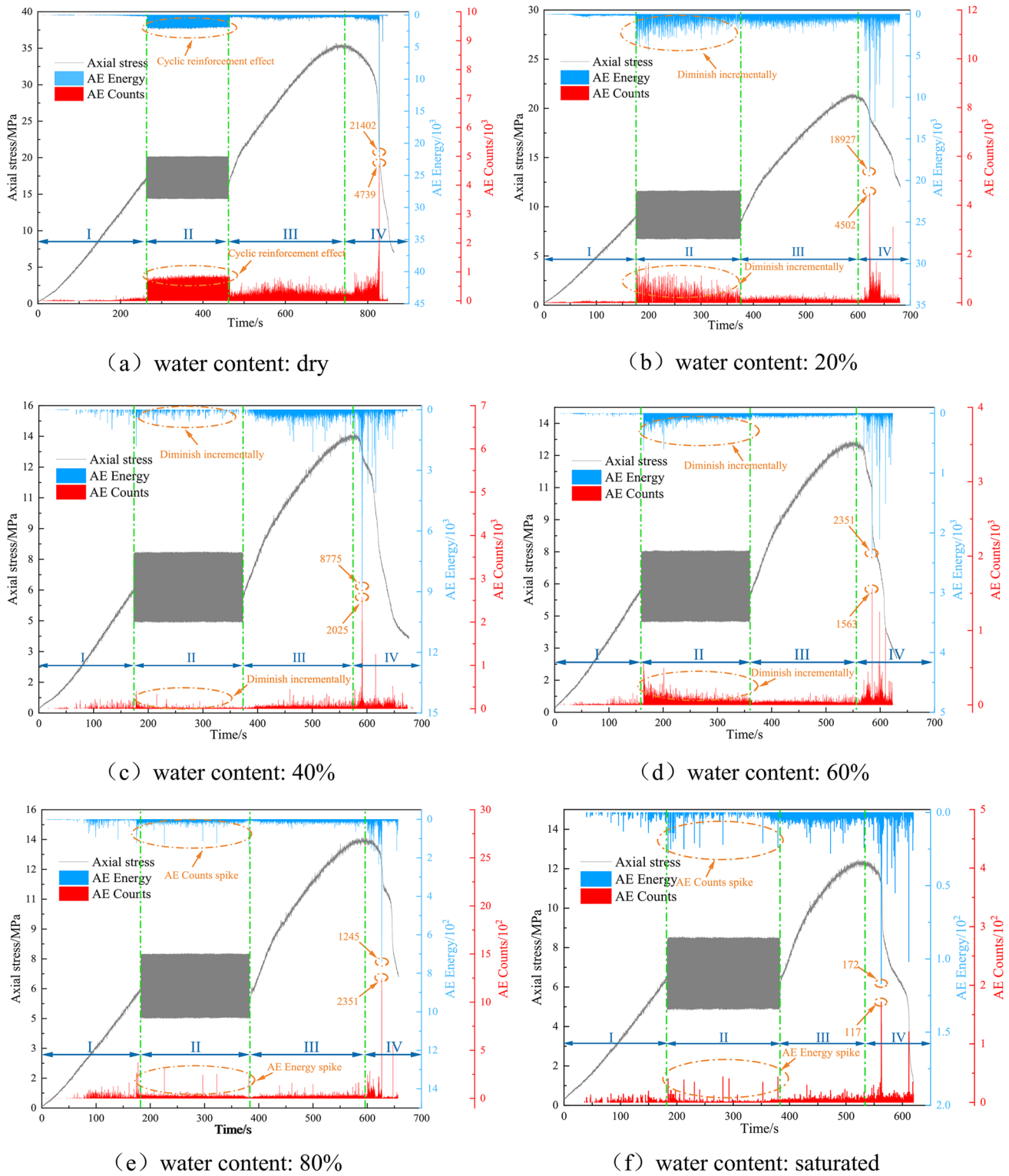
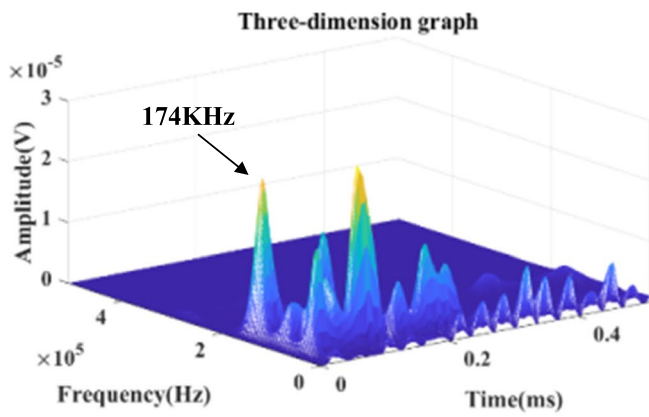


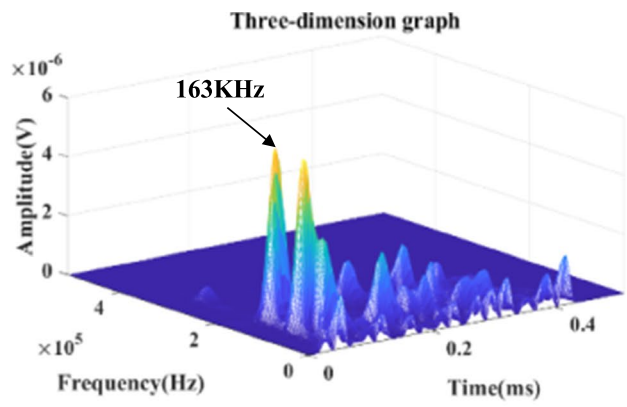
Fig.10 Acoustic emission characteristics of samples with different water contents

plot. Figure 11 shows a 3D plot of the principal frequency characteristics of the Fourier transform of the key points of the acoustic emission of rock samples with different water

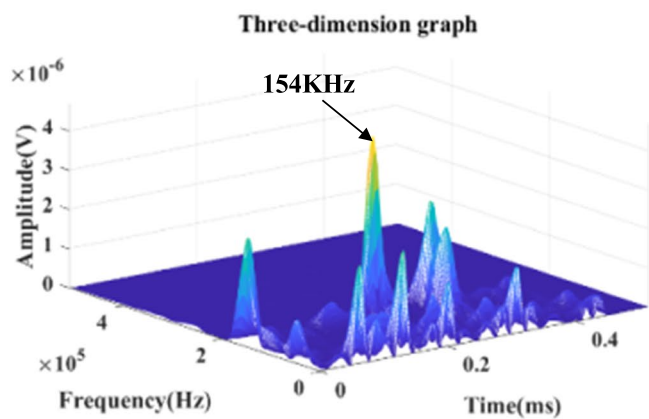
contents. The sharp peaks in the figure correspond to the dominant frequency characteristics of the acoustic emission, and the moment of sample failure is selected as the key



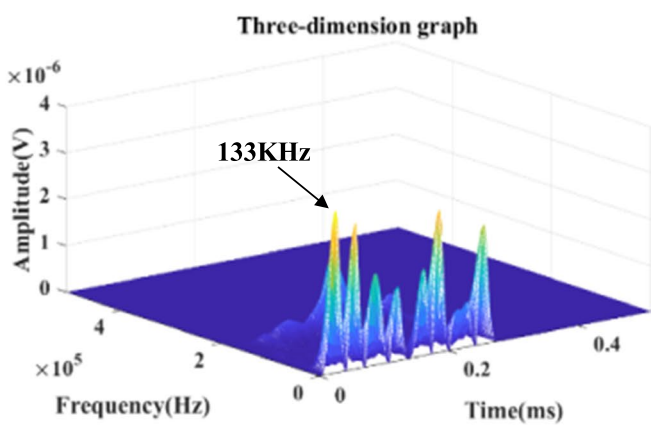
(a) water content: dry



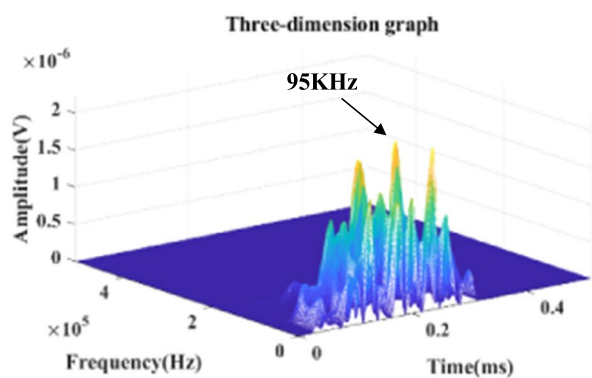
(b) water content: 20%



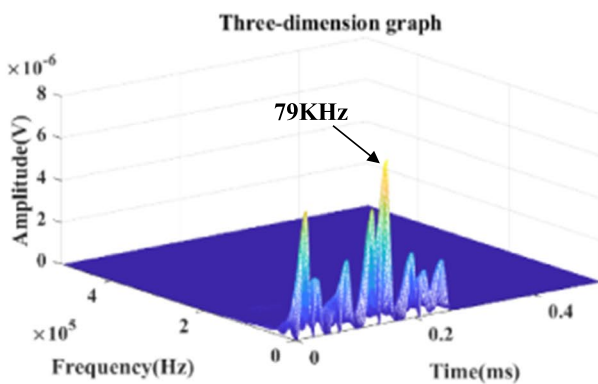
(c) water content: 40%



(d) water content: 60%



(e) water content: 80%



(f) water content: saturated

Fig.11 Amplitude-frequency-time 3D mapping

point N. The analysis reveals the following characteristics of the rock samples with different water contents: (1) The principal frequency eigenvalues of the rock sample damage decrease as the water content increases, ranging from a

maximum of 175 kHz for dry rock samples to a minimum of 79 kHz for saturated rock samples. A total of 20%–60% of the lower water content rock samples are damaged with principal frequency eigenvalues between 135 and 165 kHz,

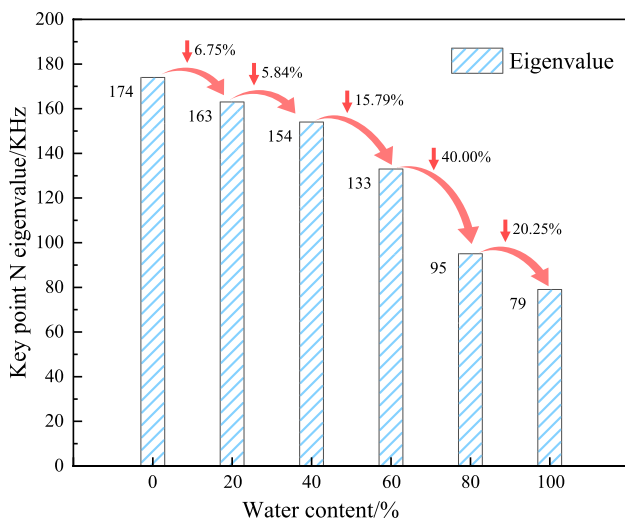


Fig. 12 Dominant frequency eigenvalues variation plot

whereas 80% of the saturated rock samples are damaged with principal frequency eigenvalues less than 100 kHz; (2) Combined with Fig. 9, it shows that the degree of damage of the rock sample increases with increasing water content decreases with increasing principal frequency eigenvalue. Thus, a higher value of the principal frequency corresponds to a lower degree of damage, whereas a lower value of the principal frequency corresponds to a higher degree of damage (Fig. 12; Table 3).

4 Conclusions

(1) Under uniaxial compression, the 20%, 40%, 60% and 80% water and the saturated rock samples show varying degrees of reduction in strength and modulus compared with the dry rock samples. The stress–strain curve of the dry rock samples falls directly after the peak, whereas the water-bearing rock samples show a stepwise rise in stress, indicating that water causes the rock to become less soft and brittle, with high plasticity. The degree of damage increases with increasing water content, and the form of damage changes from

- single bevel shear damage and ‘X’ type conjugate bevel shear damage to tunnel bottom drum type damage.
- (2) At relatively lower water content levels (60% and below), dynamic perturbation enhances the compressive strength of the samples. However, at higher water content levels (80% and above), dynamic perturbation weakens the compressive strength. Among them, the maximum strengthening effect is achieved when the water content is 20%, resulting in a 13.83% increase in comparison to uniaxial compression. The weakening effect of dynamic perturbation on samples with higher water content is not as pronounced, with the highest weakening effect observed at full saturation, amounting to only 2.47%. Compared with uniaxial compression, the form of damage in the dry rock samples remains unchanged after disturbance, whereas the water-bearing rock samples change gradually from shear damage and tensile–shear composite damage with increasing water content to more pronounced cleavage damage until saturation when they change to complete unifacial shear damage.
- (3) The evolution of acoustic emission of specimens with different water contents can be divided into static loading stage (I), dynamic loading stage (II), yield failure stage (III), and post-peak stage (IV). With the increase of water content, the number and intensity of acoustic emission signals in phase I decreased, and the number of cycles in phase II had a cyclic enhancement effect on the samples, which was more obvious in the lower water content samples, and the acoustic emission signals of the high water content samples had a sudden change in this phase. The acoustic emission energy and counting signals of the dry samples were 21,402 and 4739, respectively, while those of the saturated samples were only 117 and 172, and the acoustic emission signals decreased by multiplicative order of magnitude.
- (4) The principal frequency eigenvalues of the key points of different water-bearing rock samples decrease with increasing water content, and the degree of damage increases with decreasing principal frequency eigenvalues, corresponding to low water content—high principal frequency—low damage and high water content—low principal frequency—high damage.

Table 3 Eigenvalues (kHz) of main frequency of acoustic emission for different water content samples

Key point	Water content					
	Dryness	20%	40%	60%	80%	Saturation
N	174	163	154	133	95	79

Author contributions YJ: Writing original draft and reviewing. LC: Writing original draft and data processing. DW: Writing original draft and reviewing. HL: Checking and proofreading. GZ: Checking and proofreading. LD: Data processing. BL: Data processing and typesetting. All authors read and approved the final manuscript.

Funding This research was supported by the National Natural Science Foundation of China (No. 52204101), the Natural Science Foundation of Shandong Province (No. ZR2022QE137), Open Project of State Key Laboratory for Geomechanics and Deep Underground Engineering in CUMTB (No. SKLGDUEK2023).

Declarations

Competing interests The authors declare that they have no competing interests.

Open Access This article is licensed under a Creative Commons Attribution 4.0 International License, which permits use, sharing, adaptation, distribution and reproduction in any medium or format, as long as you give appropriate credit to the original author(s) and the source, provide a link to the Creative Commons licence, and indicate if changes were made. The images or other third party material in this article are included in the article's Creative Commons licence, unless indicated otherwise in a credit line to the material. If material is not included in the article's Creative Commons licence and your intended use is not permitted by statutory regulation or exceeds the permitted use, you will need to obtain permission directly from the copyright holder. To view a copy of this licence, visit <http://creativecommons.org/licenses/by/4.0/>.

References

- Cai X, Zhou ZL, Du XM (2020) Water-induced variations in dynamic behavior and failure characteristics of sandstone subjected to simulated geo-stress. *Int J Rock Mech Min Sci* 130:104339
- Erguler ZA, Ulusay R (2008) Water-induced variations in mechanical properties of clay-bearing rocks. *Int J Rock Mech Min* 46(2):355–370
- Feng F, Chen SJ, Zhao XD, Li DY, Wang XL, Cui JQ (2022) Effects of external dynamic disturbances and structural plane on rock fracturing around deep underground cavern. *Int J Coal Sci Technol* 9:15
- Gao LS, Xu Y, Wu BB, Wang S (2018) Dynamic compression strength of thermal damaged Fangshan marble on dry and saturated conditions. *Chin J Rock Mech Eng* 37(S2):3826–3833
- Guo YT, Zhao KL, Sun GH, Yang CH, Ma HL, Zhang GM (2011) Experimental study of fatigue deformation and damage characteristics of salt rock under cyclic loading. *Rock Soil Mech* 32(5):1353–1358
- Huang BX, Zhang N, Jing HW, Kan JG, Meng B, Li N, Xie WB, Jiao JB (2020) Large deformation theory of rheology and structural instability of the surrounding rock in deep mining roadway. *J Chin Coal Soc* 45(3):911–926
- He MC, Xie HP, Peng SP, Jiang YD (2005) Study on rock mechanics in deep mining engineering. *Chin J Rock Mech Eng* 16:2803–2813
- Li SC, Xu J, Tao YQ, Tang XJ, Yang HW (2009) Low cycle fatigue damage model and damage variable expression of rock. *Rock Soil Mech* 30(6):1611–1615
- Liu E, He S (2012) Effects of cyclic dynamic loading on the mechanical properties of intact rock samples under confining pressure conditions. *Eng Geol* 125:81–91
- Liu B, Sun YD, Yang YF, Liu XC, Bai XT, Fang TJ (2020) Strength characteristics of frozen sandstone with different water content and its strengthening mechanism. *J China Univ Min Technol* 49(06):1085–1093
- Roy DG, Singh TH, Kodikara J, Das R (2017) Effect of water saturation on the fracture and mechanical properties of sedimentary rocks. *Rock Mech Rock Eng* 50(10):2585–2600
- Sun K, Fan LM, Xia YC, Li C, Chen JP, Gao S, Wu BY, Peng J, Ji YW (2021) Impact of coal mining on groundwater of Luohe formation in Binchang mining area. *Int J Coal Sci Technol* 8:88–102
- Sun XM, Jiang M, Wang XB, Zang JC, Gang X, Miao CY (2023) Experimental study on creep mechanical properties of sandstone with different water contents in Wanfu coal mine. *Rock Soil Mech* 44(03):624–636
- Tang SB, Yu CY, Heap MJ, Chen PZ, Ren YG (2018) The influence of water saturation on the short- and long-term mechanical behavior of red sandstone. *Rock Mech Rock Eng* 51(9):2669–2687
- Wang XF, Chen XY, Wang JY, Chang ZC, Qin DD, Hang QX (2023) Creep failure mechanism and control of the deep soft rock roadway in Pingdingshan mining area. *J Min Saf Eng* 40(06):1139–1150
- Wen ZJ, Hang J, Jiang YJ, Zuo YJ, Zhu ZW, Xiao P (2021) Development and experiment of a coupled static-dynamic cyclic loading test system. *J Cent South Univ (sci Tech)* 52(8):2817–2827
- Weng L, Wu ZJ, Liu QS (2020) Dynamic mechanical properties of dry and water-saturated siltstones under sub-zero temperatures. *Rock Mech Rock Eng* 53:4381–4401
- Wong LNY, Maruvanchery V, Liu G (2015) Water effects on rock strength and stiffness degradation. *Acta Geotech* 11(4):713–737
- Xi DY, Liu XY, Zhang CY (2003) Analysis on micro and meso-damage of rock by macro-hysteresis curve. *Chin J Rock Mech Eng* 22(2):182–187
- Xiao JQ, Ding DX, Xu G, Jiang FL (2010) Deformation characteristics of rock under constant amplitude cyclic loading. *J Cent South Univ (sci Tech)* 41(2):685–691
- Xie HP, Gao F, Ju Y, Gao MZ, Zhang R, Gao YN, Liu JF, Xie LZ (2015) Quantitative definition and investigation of deep mining. *J China Coal Soc* 40(1):1–10
- Xu J, Xian XF, Wang H, Wang WZ, Yang GX (2006) Experimental study on rock deformation characteristics under cycling loading and unloading conditions. *Chin J Rock Mech Eng* 25(3):473–478
- Yang K, Zhang ZN, Chi XL, Lü X, Wei Z, Liu WJ (2022) Experimental study on crack evolution and damage characteristics of water bearing sandstone under cyclic loading. *Rock Soil Mech* 43(7):1791–1802
- Yu CH, Tang SB, Tang CA, Duan D, Zhang YJ, Liang ZZ, Ma K, Ma TH (2019) The effect of water on the creep behavior of red sandstone. *Eng Geol* 253:64–74
- Zhang QX, Ge XR, Hang M, Sun H (2006) Testing study on fatigue deformation law of red-sandstone under triaxial compression with cyclic loading. *Chin J Rock Mech Eng* 25(3):473–478
- Zhang HW, Wan ZJ, Zhao YX, Zhou CB, Zhu CQ, Lu SF (2021a) How to seal hydraulic fracturing boreholes in the large-size HDR rocks under HTHP conditions. *Lithosphere* 2021:8050488
- Zhang HW, Wan ZJ, Zhou CB, Zhao YX, Wang W, Yang YL, Teng T (2021b) High temperature mechanical properties and thermal shock effect of hot dry rock. *J Min Saf Eng* 38(01):138–145

- Zhao YX, Liu SM, Jiang YD, Wang K, Hang YQ (2016) Dynamic tensile strength of coal under dry and saturated conditions. *Rock Mech Rock Eng* 49:1709–1720
- Zhao Y, Zhou HW, Zhong JC, Liu D (2019) Study on the relation between damage and permeability of sandstone at depth under cyclic. *Int J Coal Sci Technol* 6:479–492
- Zhou H, Song M, Zhang CQ, Yang FJ, Lu XJ, Fang HG, Deng WJ (2022) Experimental study of influences of water on mechanical behaviors of argillaceous sandstone under tri-axial compression. *Rock Soil Mech* 43(9):2391–2398
- Zhang C, Qingsheng B, Penghua H, Lei W, Xiaojie W, Fangtian W (2023) Strength weakening and its micromechanism in water–rock interaction, a short review in laboratory tests. *Int J Coal Sci Technol* 10(1):10. <https://doi.org/10.1007/s40789-023-00569-6>

Publisher's Note Springer Nature remains neutral with regard to jurisdictional claims in published maps and institutional affiliations.